J. Phys.: Condens. Matter **22** (2010) 315301 (12pp) doi:10.1088/0953-8984/22/31/315301

Electrolyte solution transport in electropolar nanotubes

Jianbing Zhao[1], Patricia J Culligan[1,7], Yu Qiao[2], Qulan Zhou[3], Yibing Li[4], Moonho Tak[5], Taehyo Park[5] and Xi Chen[1,5,6,7]

[1] Department of Earth and Environmental Engineering, School of Engineering and Applied Sciences, Columbia University, New York, NY 10027, USA
[2] Department of Structural Engineering, University of California–San Diego, La Jolla, CA 92093-0085, USA
[3] State Key Laboratory of Multiphase Flow in Power Engineering, Xi'an Jiaotong University, Xi'an 710049, People's Republic of China
[4] State Key Laboratory of Automotive Safety & Energy, Department of Automotive Engineering, Tsinghua University, Beijing, 100084, People's Republic of China
[5] Department of Civil and Environmental Engineering, Hanyang University, Seoul 133-791, Korea
[6] School of Aerospace, Xi'an Jiaotong University, Xi'an 710049, People's Republic of China

E-mail: pjc2104@columbia.edu and xichen@columbia.edu

Received 11 April 2010, in final form 10 June 2010
Published 9 July 2010
Online at stacks.iop.org/JPhysCM/22/315301

Abstract
Electrolyte transport in nanochannels plays an important role in a number of emerging areas. Using non-equilibrium molecular dynamics (NEMD) simulations, the fundamental transport behavior of an electrolyte/water solution in a confined model nanoenvironment is systematically investigated by varying the nanochannel dimension, solid phase, electrolyte phase, ion concentration and transport rate. It is found that the shear resistance encountered by the nanofluid strongly depends on these material/system parameters; furthermore, several effects are coupled. The mechanisms of the nanofluidic transport characteristics are explained by considering the unique molecular/ion structure formed inside the nanochannel. The lower shear resistance observed in some of the systems studies could be beneficial for nanoconductors, while the higher shear resistance (or higher effective viscosity) observed in other systems might enhance the performance of energy dissipation devices.

(Some figures in this article are in colour only in the electronic version)

1. Introduction

The rapid development of new technologies for drug delivery, sensing, energy conversion and storage, environmental and biomedical science and engineering [1–3] have drawn increasing attention to the need for understanding ion transport behavior in nanoenvironments [4, 5]. In biological systems, numerous nanoscale conductors on the cell membranes function as ion channels and ion pumps to create an ion concentration gradient across the cell membrane. The established ion gradients then provide an energy source to pump nutrients into the cells via ion channels and other transport proteins [6–8]—such a process is essential to many of life's functions, including the electrical signaling in nerves, muscles and synapses, and a cell's maintenance of homeostatic balance [9–11]. In the past decade, a large number of fundamental experimental and computational studies have been carried out to obtain an improved knowledge of nanofluidic/ion transport, which could in turn provide a firm foundation for the development of the aforementioned advanced techniques [12–14].

Progress in the area of nanofluidics is also enabling the development of high-performance nanoporous energy absorption systems (NEAS) [15]: by applying an external pressure to force non-wetting liquids to intrude into hydrophobic nanopores, the external mechanical energy is partially converted into the energy associated with the liquid–

[7] Authors to whom any correspondence should be addressed.

solid interface to change the thermodynamic status of the intrusive liquid, and partially dissipated via the extensive solid–liquid interface friction (so as to sustain the transport of the liquid in the confined nanoenvironment). Owing to the ultrahigh specific surface area of the nanoporous material, the energy absorption efficiency of NEAS can be orders of magnitude higher than conventional systems [15].

The surface hydrophobicity and confinement level of nanopores are crucial to the thermodynamic status during the intrusion/extrusion process of liquid in nanopores [16]. For energy absorption applications, two critical variables govern the performance of NEAS: the first one is the intrusion pressure beyond which the liquid may invade the hydrophobic nanopores [17]: this is the working pressure and it also partially governs the energy absorption density. The second is the energy dissipation during the transport process of the (continuous) invaded liquid, and this term predominates the energy absorption capability, especially when the nanopore is relatively long [18]. The focus of this paper is the transport process following liquid intrusion.

Previous numerical and experimental research has shown that the nanofluidic transport behavior (and thus the performance of NEAS) is affected by several material and system parameters, such as the surface hydrophobicity and confinement level of nanopores [16, 19], composition of the solid phase (e.g. silica, zeolite, carbon) [20–22], treatment of nanopore surfaces [23, 24], base constitutions of liquids [25, 26] and the addition of chemicals with varying concentrations [27, 28], liquid transport/loading rate [18, 29] and the presence of gas phases [30, 31], among others. While these characteristics offer flexibility for fine tuning the performance of NEAS, the mechanisms affecting nanofluidic properties must be clearly understood.

At the nanoscale, the conventional continuum fluid model usually breaks down, and the friction at the liquid–solid interface from the direct interaction between liquid and solid phases strongly affects the nanofluidic transport behavior. To gain a basic knowledge, atomistic simulations of nanofluids in a neutral carbon nanotube (CNT) were carried out by a few researchers [32, 33]. To provide a qualitative description of fundamental liquid–solid interactions, the effective shear stress and effective shear viscosity [18, 34] were introduced, and both of these measures were found to decrease with increasing concentration of electrolytes (when the pore size is unchanged) and decrease with reduced nanotube sizes (when the transport rate remains fixed). Although these findings in a neutral CNT are consistent with experiments on a nanoporous carbon, it remains unclear whether they may be extended to electropolar nanotubes: in an electropolar nanotube, the pore surface atoms carry positive or negative charges, which could significantly affect the interaction between solid phase and polar water molecules, especially when ions are also present in the nanofluid [27, 28, 35, 36]. In essence, in a neutral nanotube the van der Waals interaction governs the shear stress, whereas in an electropolar nanotube the electrostatic force exerts substantial influence. Subsequently, the fundamental nanofluidic behavior may be quite different when an electropolar nanotube is employed. Note that electropolar nanoporous solids, such as nanoporous silica and zeolite, are more frequently used in high-performance NEAS [15, 18, 36] than their nonpolar counterparts. Therefore, it is also of practical importance to systematically investigate the transport behaviors in electropolar nanopores, to better guide the development of NEAS with optimized energy absorption properties.

In this paper, we extend our previous work [18, 34] to investigate the transport behaviors and intrinsic mechanisms of electrolyte solutions confined in model electropolar nanotubes using non-equilibrium molecular dynamics (NEMD) simulations. In order to explore the general mechanical characteristics of fluidic transport in electropolar nanotubes and avoid the complexity of actual nanopore surface features, rigid model nanotubes with 'ideally' smooth surfaces (and without any chemical groups or net electric charges on the surface) are adopted in the current study. Although this assumption may be overly simplified, the model nanotubes are envisioned to lead to insights about certain fundamental mechanical behaviors of solid–liquid interactions in confined nanoenvironments and provide valuable guidelines for developing nanofluidic devices, such as NEAS.

The numerical models of polar nanotubes are created with negative and positive electric charges alternately presenting on element atoms. Several metal oxides, such as SiO_2, ZnO and Al_2O_3, are selected to represent different examples of solid phase constitutions. Special emphasis is placed on the SiO_2 nanotube since it, to some extent, resembles the nanoporous zeolite or silica [37, 38]. Representative electrolytes, including KCl, NaCl and LiCl, are employed to explore the ion size effect and concentration effect. This study on the fundamental nanofluidic behavior, in particular the variation of the shear stress and effective shear viscosity, will provide useful insights for enhancing the energy absorption performances of NEAS by optimizing relevant material and system parameters (such as the phase and size of nanopores, and type and concentration of ions, transport/loading rate, etc), as well as for other applications of nanofluids.

2. Computational method

2.1. Model and force field

In a model electropolar nanotube, the nonbond potentials govern the interaction between solid and liquid atoms/molecules. The van der Waals and electrostatic interactions under consideration are described by the Lennard-Jones potential (12-6) and Coulombic potential, respectively. To study the size dependence of transport behaviors, the nanopore diameter (D) is varied from 0.81 to 10 nm (for simplicity the nanopores are taken to be straight and rigid; the effect of pore surface structure and pore compliance will be explored elsewhere). In particular, model SiO_2 nanopores with diameters of 0.81 and 2.51 nm that best match the pore size of nanoporous zeolite (MFI) and MCM-41 silica gel in parallel experiments [39, 40], respectively, are our main focus. Transport behaviors of LiCl–, NaCl– and KCl–water solutions are simulated with their molar concentrations varying from 1.0 to 4.0 M ($M = 1.0\ \mathrm{mol\,l^{-1}}$) to introduce both ionic concentration and ion size effects. In

Table 1. Lennard-Jones potential parameter used in MD simulations.

Ion/atom	ε (kcal mol^{-1})	r^0 (Å)	q (e)
Li^+	0.7214	3.4518	1.0
Na^+	0.738	3.9624	1.0
K^+	0.7441	4.8858	1.0
Cl^-	0.305	3.915	−1.0
Al^{3+}	0.7936	2.669	0.6675
Zn^{2+}	0.2166	2.228	0.445
Si^{4+}	0.19	4.45	0.89
O^{2-}	0.24	3.535	−0.445
O^{-2} [a]	0.2848	3.6001	−0.8476
H^+			0.4238

[a] Stands for the oxygen atom in water molecules.

addition to the model SiO_2 nanotube, nanofluidic phenomena in model ZnO and Al_2O_3 nanopores are also examined to reveal the solid phase dependences, as well as to generalize the characteristics of transport rate effects in electropolar nanopores.

The water molecules are described by the empirical rigid intermolecular-potential three-point (TIP3P) model [41, 42]. The nonbonding ion–solvent, ion–wall and solvent–wall interactions, i.e. van der Waals and Coulomb interactions, are described by the Lennard-Jones (12-6) and Coulombic potentials, respectively. It is worth noticing that the Morse potential could also be used to account for the van der Waals interaction; however, the Morse approximation would insignificantly underestimate the repulsive energy and overestimate the attractive energy when the intermolecular distance deviated from the equilibrium state [43]. In view of this reason and also in an attempt to remain consistent with previous studies [18, 34] and to be comparable with published benchmark simulations from other researchers, the Lennard-Jones water model is still preferentially adopted in the presented study.

In our simulations, to handle the long range Coulomb interactions, the particle–particle particle-mesh technique (PPPM) is adopted with a root mean square accuracy of 10^{-4} [44]. The interionic potential E_{ij} used for the additive ions is of the Huggins–Mayer form [45]: $E_{ij}(r) = q_i q_j/r + B_{ij}e^{-r/\rho_{ij}} - C_{ij}/r^6$, in which q_i is the charge of the ith ion, r the distance between ion pairs, and B_{ij} and C_{ij} the potential coefficients. The values of the above potential parameters are listed in tables 1 and 2 [46–49].

2.2. Simulation procedure

The length (in the axial direction of the nanotube) of the simulation cell is $L = 320$ Å and its lateral dimension is appropriately set to simulate an isolated nanochannel. The number of water molecules, N, is chosen such that the averaged water density inside the occupied volume[8] is close to its bulk value of 998 kg m^{-3}. In the initial stage, certain water molecules are replaced by ions (such as Na^+ or Cl^-) to reach a desired concentration of the electrolyte, shown in figure 1.

[8] The occupied volume is a cylindrical space: its diameter at equilibrium can be approximated as $D^* = (D + D^L)/2$, where D is the diameter of the solid nanotube and D^L is the diameter of the water segment in which 95% of the transported liquid was contained. D^* can be regarded as the effective diameter of the 'interface' between solid and liquid phases.

Table 2. Parameters for solute–solvent potential.

Parameter	Value	Parameter	Value
ε_{ONa^+}	0.4324 kcal mol^{-1}	$\varepsilon_{O^*Na^+}$	0.3367 kcal mol^{-1}
$r^0_{ONa^+}$	3.8057 Å	$r^0_{O^*Na^+}$	3.8011 Å
$\varepsilon^0_{OCl^-}$	0.2806 kcal mol^{-1}	$\varepsilon^0_{O^*Cl^-}$	0.2185 kcal mol^{-1}
$r^0_{OCl^-}$	3.7770 Å	$r^0_{O^*Cl^-}$	3.7722 Å
q_{Na^+}	+1.0 e	$\varepsilon^0_{SiNa^+}$	0.3529 kcal mol^{-1}
q_{Cl^-}	−1.0 e	$r^0_{SiNa^+}$	4.2409 Å
$B_{Na^+Na^+}$	9769.55 kcal mol^{-1}	$\varepsilon^0_{SiCl^-}$	0.2239 kcal mol^{-1}
$\rho_{Na^+Na^+}$	0.317 00 Å	$r^0_{SiCl^-}$	4.2243 Å
$C_{Na^+Na^+}$	24.172 kcal mol^{-1} Å^{-6}	$\varepsilon^0_{AlNa^+}$	0.7653 kcal mol^{-1}
$B_{Cl^-Cl^-}$	80 285.8 kcal mol^{-1}	$r^0_{AlNa^+}$	3.3157 Å
$\rho_{Cl^-Cl^-}$	0.317 00 Å	$\varepsilon^0_{AlCl^-}$	0.4920 kcal mol^{-1}
$C_{Cl^-Cl^-}$	1683.4 kcal mol^{-1} Å^{-6}	$r^0_{AlCl^-}$	3.292 Å
$B_{Na^+Cl^-}$	28 920.2 kcal mol^{-1}	$\varepsilon^0_{ZnNa^+}$	0.3998 kcal mol^{-1}
$\rho_{Na^+Cl^-}$	0.317 00 Å	$r^0_{ZnNa^+}$	3.0952 Å
$C_{Na^+Cl^-}$	161.15 kcal mol^{-1} Å^{-6}	$\varepsilon^0_{ZnCl^-}$	0.2570 kcal mol^{-1}
		$r^0_{ZnCl^-}$	3.0715 Å

The simulations are performed using LAMMPS [50, 51] with a time step of 1.0 fs. A periodic boundary condition is applied in the axial direction to mimic transport inside an infinitely long channel. The temperature is maintained at 298.5 K by using a Nose/Hoover thermostat with a time constant of 0.1 ps. To avoid artificial heating caused by the imposed axial displacements, the mean axial velocity of the liquid mass center is subtracted from the axial component of the velocity of each liquid molecule during the calculation of temperature.

After initialization, an NVT simulation is first performed for 100 ps to minimize the system energy. After full relaxation, a strong gravitational force field (which is different and much larger than the Earth's gravity), with magnitude $m_i\tilde{g}$ (where m_i is the mass of the ith particle), is artificially applied on each molecule in the axial direction of the tube to initiate the flow, and the NVE ensemble is employed to monitor the velocity of water molecules. When the average transport rate of the liquid molecules (i.e. the flow rate, see below) reaches a desired value, the applied gravitational force field is removed and the liquid is allowed to freely decelerate. The real-time transport velocity is recorded to identify an initial linear decelerating window, in which the magnitude of transport velocity is allowed to drop by a certain small percentage; at the same time, the system temperature is closely monitored to make sure that there was no sudden rise in system temperature. After completing sampling of the flowing variables, the deceleration $\bar{a}$ can thus be computed and the effective shear stress at the liquid–solid interface can be obtained as $\tau = \sum m_i\bar{a}/\pi D^*L$, where $\sum m_i$ is the summation of the liquid mass in the nanotube, including water and ions, and D^* is the effective diameter of the transport nanotube (see footnote 8). τ is a function of the flow rate and tube size, as well as the liquid

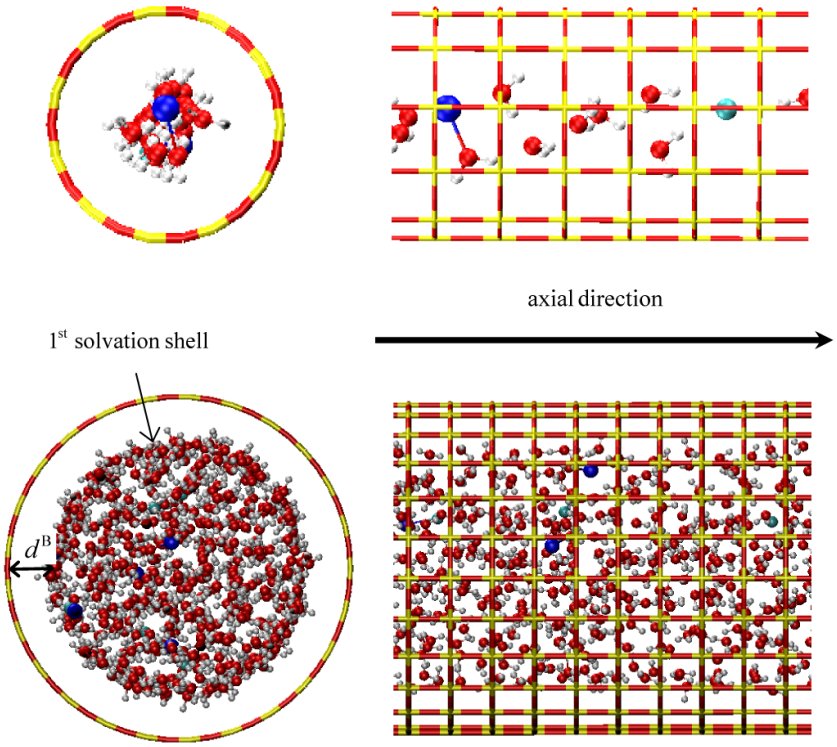

Figure 1. Snapshots of the configuration of NaCl and water solution (3.0 M) inside the SiO_2 model nanotubes. Top: 8.61 Å for the nanotube's diameter; bottom: 25.1 Å for the nanotube's diameter.

and solid phases [52]. As an effective interpretation of the nanotransport behavior, the phenomenological definition of the effective shear viscosity $\tilde{\eta}$ follows our previous studies [18, 34] as $\tilde{\eta} = \tau R/(4\bar{v})$, where $R = D^*/2$ is simply taken as the radius of the nanopores and $\bar{v}$ is the averaged transport (flow) rate.

3. Results and discussion

3.1. Fluid behavior in a model SiO_2 nanotube

3.1.1. Tube size effect. We first focus on the model SiO_2 nanotube, which may provide some useful insights on the nanoporous silica or zeolite used in parallel experiments [40, 53]. Figure 1 shows the different configurations of water molecules inside two ideal numerical models of polar nanotubes with typical diameters $D = 0.81$ nm (small) and $D = 2.51$ nm (medium)[9]. With different pore radii, the distinct confinements from the solid wall strongly affect the distribution of liquid molecules: a single water molecule chain is formed in the small SiO_2 model nanotube ($D = 0.81$ nm), instead of a 'layered' structure observed in the medium size nanotube ($D = 2.51$ nm). This distribution significantly influences the repulsive force imposed by the solid wall during the nanofluidic transport and thus dominates the shear transport stress [18, 34].

The quantitative tube size effect is now examined (with 2.0 M NaCl–water solution and a fixed transport rate of ~200 m s^{-1} [18]). Figure 2 shows the variations of the effective shear stress τ and effective shear viscosity $\tilde{\eta}$ as functions of the nanotube diameter (solid lines), with diameters ranging from 0.81 to 10.0 nm. Both the shear stress and effective shear viscosity get smaller as the pore size is reduced; a similar decreasing trend is found in neutral CNTs (dotted lines in figure 2, which is consistent with the knowledge from the literature that water flow through a small CNT can be ultrafast [32, 33]). Note that, when the tube radius is given, the magnitudes of both shear stress and effective viscosity are much larger in an SiO_2 model nanotube than that in a CNT (although the viscosity in both nanotubes is still much smaller than that of bulk water). Compared with the neutral CNT, the larger shear stress and effective shear viscosity in the SiO_2 model nanotube are caused by the extra electrostatic interaction between the polar nanotube wall and the charge-enhanced liquid. The MD simulations show that such an interaction draws the first solvation shell closer to the wall and thus greatly increases the transport resistant force in comparison to that in the neutral channel [34].

3.1.2. Ion concentration and ion size effect. Under a given transport rate (~200 m s^{-1}) and medium polar nanotube

[9] It is remarked again that the ideal polar nanotube numerical model is only intended to reflect the essential physical properties of the nanopore, i.e. dimension, solid phase compositions, etc. By employing such a simplified model with an 'ideally' smooth and rigid pore surface, we hope to circumvent the complex geometrical structure of the actual nanopore and only focus on the more basic nanofluidic transport behavior. Of course, there is no doubt that the 'practical' factors including the geometrical shape of the nanopore, the solid surface roughness, the tortuosity of the pore inner space, the chemical groups that deposit on the nanopore solid surface, deformability of the pore wall, etc, would affect the nanofluid transport behavior—the effects of these factors will be studied in more detail in future.

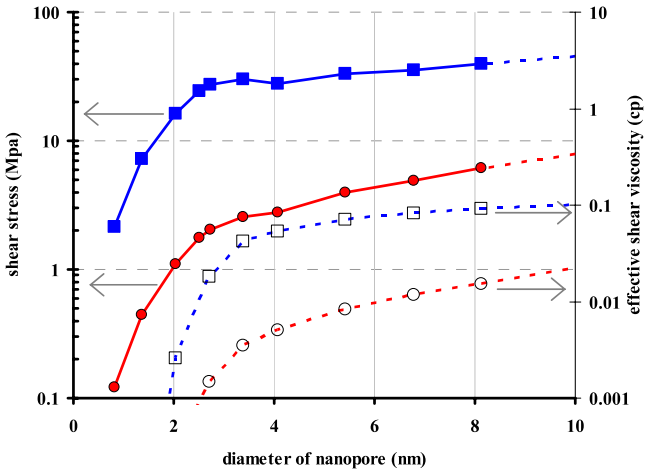

Figure 2. Distributions of shear stress (SiO_2 model nanotube: solid blue line with filled square symbol; CNT: red solid line with filled circle symbol) and effective shear viscosity (SiO_2 model nanotube: blue dot line with unfilled square symbol; CNT: red dotted line with unfilled circle symbol) as functions of nanopore diameters. The above results were obtained from 2.0 M NaCl–water transport, with the simulation conducted at a transport rate of ∼200 m s^{-1}.

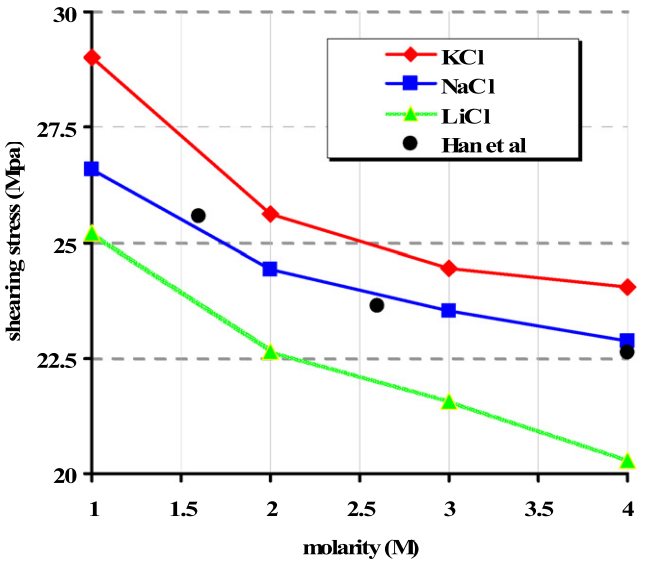

Figure 3. Shear stress distributions as a function of electrolyte molar concentration in the polar SiO_2 model nanotube with a diameter of 2.51 nm and transport rate of ∼200 m s^{-1}. The ● stands for the experimental results obtained from Han *et al* [40].

diameter (2.51 nm), figure 3 presents the decreasing trend of the effective shear stress with increasing concentration of electrolyte inside the model SiO_2 nanotube, which is again similar to that in a neutral CNT [34]. Taking the KCl–water solution for example, the shear stress decreases by around 17% as the molar concentration increases from 1.0 to 4.0 M. Comparing with the neutral CNT [34], the shear stress in the polar model SiO_2 nanotube is almost one order of magnitude higher. The ion size effect is also apparent: when the molar concentration is fixed at 2.0 M, the shear stresses for the three electrolyte solutions are $\tau_{LiCl} \approx 22.6$ MPa, $\tau_{NaCl} \approx 24.4$ MPa and $\tau_{KCl} \approx 25.7$ MPa, respectively, which echo the fact that the larger ionic size leads to a stronger transport shear stress, since the ionic size φ of these three ions follows the order of $\phi^{Li^+} < \phi^{Na^+} < \phi^{K^+}$.

Nonetheless, the transport characteristics are very different in the smaller, molecular-sized polar nanotube ($D =$ 0.81 nm). In figure 4, the effective shear stress seems to increase with the molar concentration of LiCl, NaCl and KCl. Taking the transport of KCl solution as an example, the magnitude of effective shear stress changes from 2.5 to 5.2 MPa as the electrolyte concentration increases from 1.0 to 4.0 M. In spite of the contradictory trend with electrolyte concentration, the ion size effect still holds in the small nanochannel, where the shear stresses of different electrolytes follow the order of $\tau_{KCl} > \tau_{NaCl} > \tau_{LiCl}$.

For both sizes of nanopores, the simulation results are qualitatively compared with experimental results [40, 53], with the results in figure 3 being compared with experiments on an MCM-41 silica gel (with NaCl solution), and those in figure 4 being compared with tests on a zeolite beta (with KCl solution). Despite the surface structural difference between the ideal model tube and the real nanopore used in experiments, the trends revealed in MD simulations are in reasonable agreement with the experimental results. The next question is: why is the

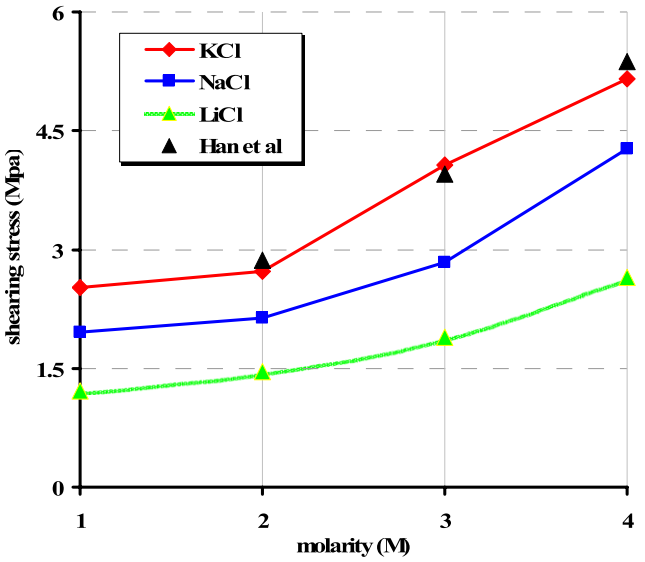

Figure 4. Shear stress distributions as a function of electrolyte molar concentration in the polar SiO_2 model nanotube with a diameter of 0.81 nm and transport rate of ∼200 m s^{-1}. The ▲ stands for the experimental results from Han *et al* [53].

trend of shear stress versus molar concentration reversed in the molecular-sized polar nanopore?

In order to answer this question, the configurations of liquid molecules (only NaCl is illustrated below) through the cross section of the nanotubes are examined, as presented in figures 5–8. We first investigate the nanotube with medium or larger sizes, and use $D = 2.51$ nm as an example. The radial distributions of water molecules in the medium and small SiO_2 nanopores, along with the electrolyte solution concentrations, are provided in figure 5(a). Inside the medium or larger size polar nanotube, a layered structure of liquid

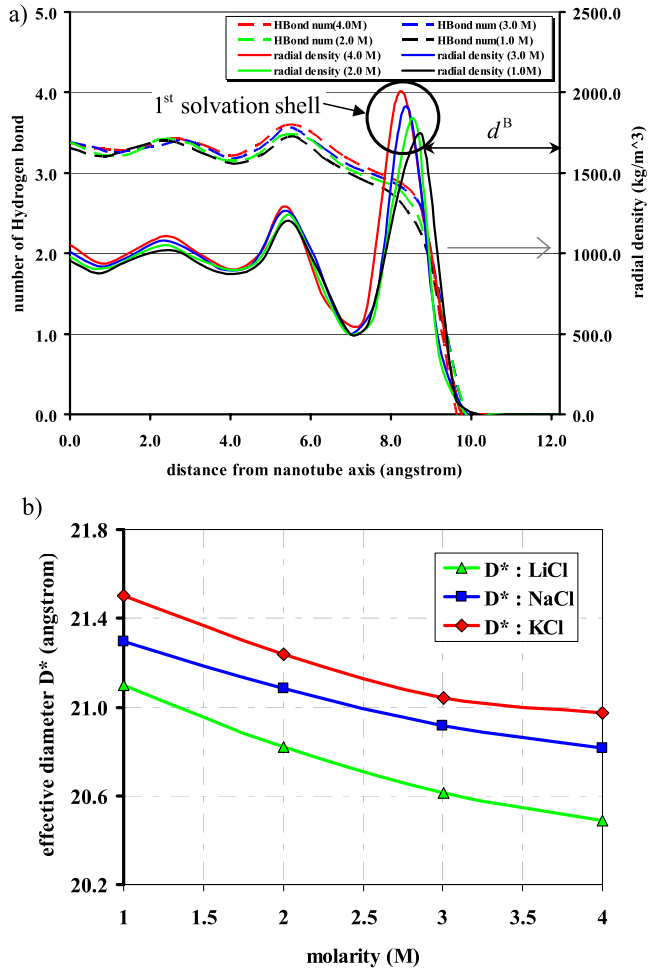

Figure 5. (a) Variation of the radial density of water in the SiO_2 model nanotube ($D = 2.51$ nm) and the number of hydrogen bonds, at the transport rate of ∼200 m s^{-1}; (b) the corresponding variations of effective D^* as functions of electrolyte molar concentration.

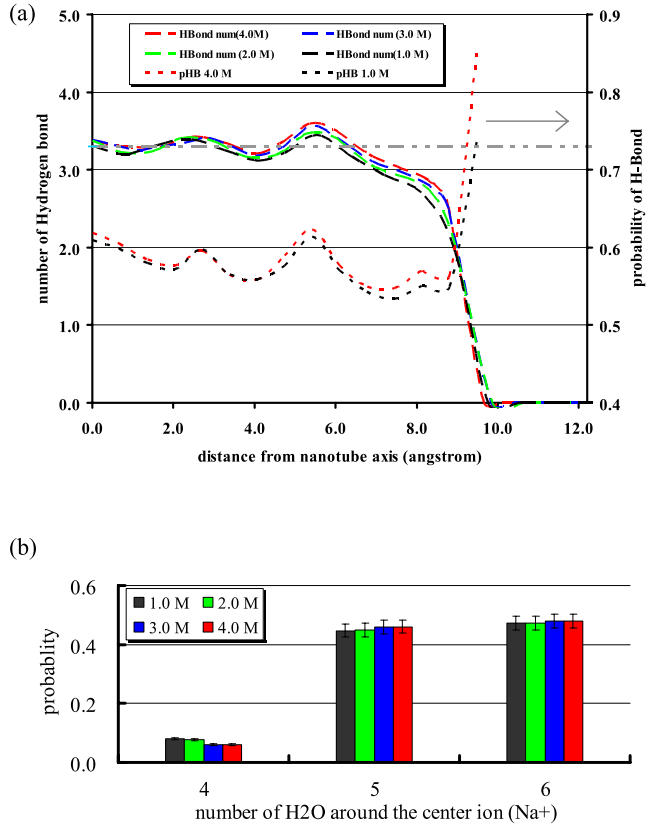

Figure 6. Medium nanopore behavior: (a) radial distribution of the hydrogen bond number n_{HB} and bonding percentage p_{HB}. (SiO_2 model nanotube, $D = 2.51$ nm) at the transport rate of ∼200 m s^{-1}. The gray dashed–double dotted line indicates a reference number of 3.3. The value of n_{HB} for bulk water at room temperature is found to be approximately 3.63 in our MD simulations. (b) The probability distribution of the number of water molecules around the sodium ion (within a distance of 3.2 Å).

molecules forms among which the first solvation shell closest to the wall has the maximum density, figures 1 and 5. At equilibrium, the distance between the first solvation shell (see figure 1, for example) and the solid wall is denoted as d^B. From the distribution of the radial density, as shown in figure 5(a), it is apparent that both the density magnitude and the equilibrium distance d^B strongly depend on the electrolyte concentration. As the molar concentration increases from 1.0 M to 4.0 M, the magnitude of d^B monotonically increases and that also causes a higher liquid density at the first solvation shell and noting the fact that among molecules/atoms, the short range repulsive force in the Lennard-Jones potential, the long range attractive force and the Coulombic force electric force decays with increasing d^B. During fluidic transport in nanotubes, a certain number of liquid molecules/ions with higher kinetic momentum from the mainstream may collide with solid wall atoms; subsequently, under the influence of repulsive force from solid wall atoms, they may rebound back to the mainstream of liquid molecules/ions. During this process, kinetic momentum is exchanged between liquid and solid phases and the shearing stress is induced. Consequently, the repulsive force field between liquid molecules/ions and solid wall atoms quickly decays with just a small increment in d^B, which may dominate over others with respect to transport resistance, and thus the decreasing trend of the effective shear stress τ with elevated electrolyte concentration should be reasonably expected. Although a larger d^B at a higher concentration means more coherent clusters of water molecules and higher density magnitude at the first solvation shell (figure 5(a)), this increased density is, at most, a function of $1/r_{ij}^2$ and ineffective to convert the above decreasing trend of τ with molar concentrations of chemicals.

More specifically, figure 5(b) illustrates the variations of the previously defined effective diameter D^* as a function of the electrolyte molar concentration, for KCl–, NaCl– and LiCl–water solutions, respectively. The magnitudes of D^* for these three electrolytes underpin the ionic size effect discussed above in section 3.1.2. The bigger size of ion, i.e. the K^+ cation, requires more accommodation space, and so do the solvation shells formed by them and their surrounding water molecules. As a consequence, the first solvation shell's position is forced to be closer to the solid wall. Moreover, for larger cation its electrostatic interaction with the solid wall is strengthened, and thus it is reasonable to see a stronger

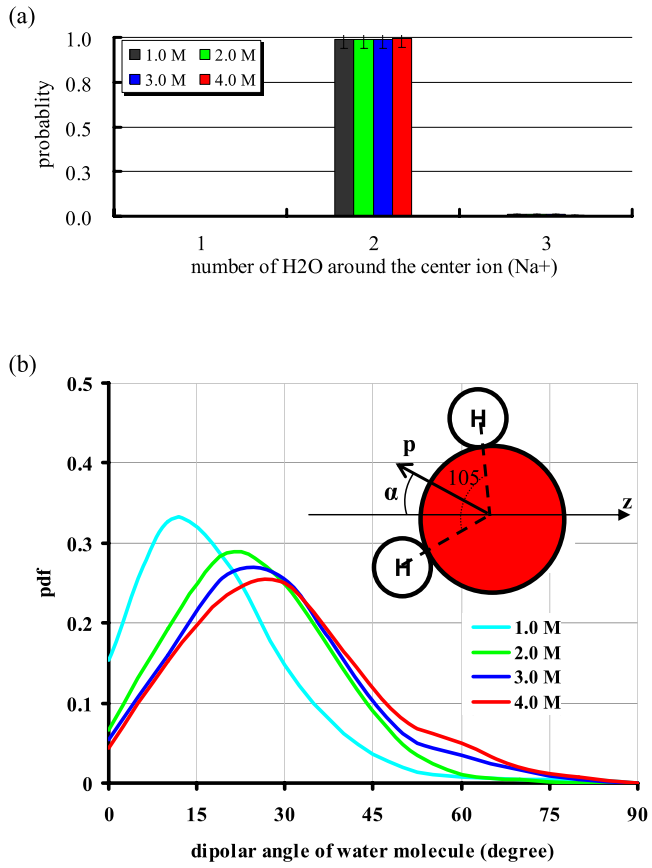

Figure 7. Small nanopore behavior: (a) the probability distribution of the number of water molecules around the sodium ion (within a distance of 3.2 Å from the ion) and (b) probability distribution function of the dipole angle α of water molecules to the nanotube axial direction z, in the SiO_2 model nanotube ($D \approx 0.81$ nm) at the transport rate of $\sim$200 m s^{-1}. The electrolyte solution used in this example is NaCl. The outward movement of peak position with increasing molar concentration indicates stronger perturbation of electrolyte due to the increasing presence of ions in water.

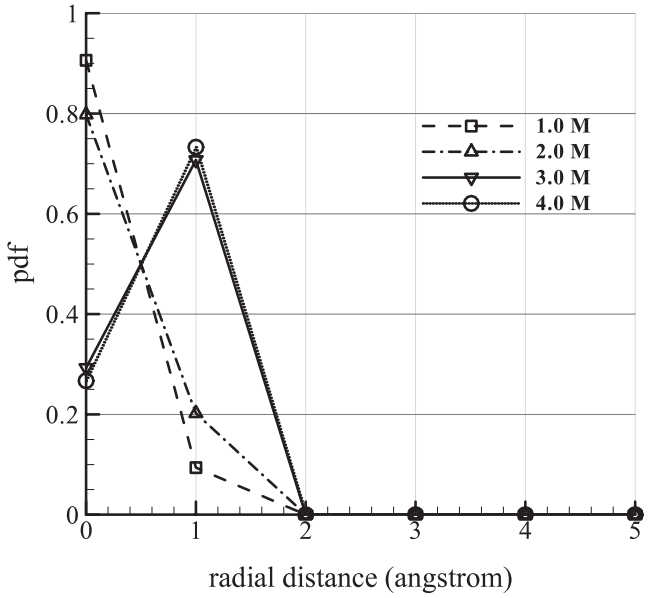

Figure 8. Probability distribution of water molecules as a function of the distance to the axis of the SiO_2 model nanotube ($\bar{v} \approx 200$ m s^{-1}) at different molar concentrations of electrolyte, e.g. NaCl.

transport resistance (comparing with LiCl-and NaCl-based water solution systems). Also according to figure 5(b), at the same molarity, the absolute difference between each case is minor. For example, at 1.0 M electrolyte concentration, the D^* in the case of an NaCl–water solution is 0.97% larger than that in a LiCl–water solution, while the D^* turns out to be 0.91% smaller than that in the KCl–water solution. In spite of such a trivial change in D^*, its ultimate effect on the transport-resistant stress is substantial, since larger D^* exposes more liquid molecules/ions to interaction with thr solid wall.

To further clarify the relation between shearing transport resistance and electrolyte–water solution concentration, the interaction among the water molecules is examined by analyzing the distribution of the hydrogen bonds and their correlation with the varying electrolyte concentration. The hydrogen bond (HB) plays a crucial role in determining the various properties of water, e.g. viscosity, surface tension and temperature dependence of density [19, 54, 55]. In this study, two water molecules are considered to be hydrogen-bonded if (a) the O–O distance is less than 3.5 Å and (b) the O–H$\cdots$O angle (hydrogen bond angle θ_{HB}) is less than 30° [56].

In bulk water, the number of hydrogen bonds per water molecule n_{HB} at the room temperature of 298.5 K was found to be about 3.63 in our MD simulation (consistent with the literature [54]). In the present study, inside the medium sized SiO_2 tube of diameter 2.51 nm, n_{HB} is calculated to be smaller (with an average n_{HB} close to 3.3), figures 5 and 6; this difference may be partially attributed to the presence of additive ions, while the major cause should be due to the nanoscale confinement. At the liquid–solid interface, due to the presence of the solid wall, one of the hydrogen bonds of the water molecules is broken and the average n_{HB} is reduced to 2.59 at the first solvation shell. When moving toward the center of the nanotube, the hydrogen bond number increases and reaches a peak value near the position of the second solvation shell, after which the distribution of n_{HB} gradually converges (but smaller than that of bulk water).

In figure 6(a), the percentage of hydrogen bonds, p_{HB}[10], which characterizes the hydrogen bonding pattern of the water molecules, is calculated to show the effects of electrolyte concentration (dashed lines in figure 6(a), where the NaCl solutions are 1.0 M and 3.0 M in molar concentration, respectively). For both concentrations, near the solid wall due to the highly compacted water molecules, the percentage of hydrogen bonds can be as high as over 80%. The higher concentration of electrolyte increases the value of p_{HB}, suggesting that the water molecules are more coherent, which could reduce flow resistance and facilitate the transport of the electrolyte solution in the medium sized polar nanotube. Moreover, if we examine the averaged water molecule number in the first solvation shell of Na^+ (n_{H2O}, calculated in a region

[10] The bonding percentage is defined as $p_{HB} = n_{HB}/n_{r=0.35\ nm}$, where n_{HB} is the number of water molecules that are hydrogen-bonded to a given molecule and $n_{r=0.35\ nm}$ is the total number of water molecules that are within 0.35 nm from the given water molecule.

within 3.2 Å from the center of the cation [57]), a slightly increasing trend of n_{H2O} around the Na^+ can be identified as the NaCl mole concentration is increased from 1.0 to 4.0 M. This tendency may serve as increased evidence that, in a highly confined nanoenvironment, with more ions present in the electrolyte solution, the liquid appears to be more 'coherent'.

The above analyses are specifically for the medium sized SiO_2 model nanotube with $D = 2.51$ nm. In the molecular-sized nanotube ($D = 0.81$ nm as an illustrative example), a quasi-one-dimensional chain of water molecules is formed and the molecular structure is quite different from that in larger pores [16]. As the water molecules invade into the nanopores, two of the hydrogen bonds may be deprived [19] and thus the 'continuous' radial density profile and H-bond number distribution are no longer accurate indicators of the coherence among water molecules in such a highly confined nanoenvironment. Indeed, in such a small space, on average only two water molecules are allowed within 'the first solvation shell' for the current range of electrolyte concentrations investigated [58] (figure 7(a)). Therefore, no more information on the transport behavior could be extracted from the distribution function of water molecules and ions in the molecular-sized tube.

As an alternative approach, we explore the probability distribution of water molecules in the molecular-sized nanotube, in terms of the dipole angle of water molecules and the positions of water molecules from the centerline of the nanotube. The dipole angle is the angle between the axis of the nanotube and the dipole moment vector of the water molecule [59], given as a function of electrolyte molar concentration in figure 7 ($D = 0.81$ nm). When the molar concentration is relatively low, e.g. 1.0 M, most dipole angles are smaller than 15°, and almost all of the water molecules are located close to the centerline of the nanotube, figure 8. With fewer ions, the motion of water molecules is less perturbed and they prefer to stay near the center axis of the nanotube to reduce potential energy. In this case, the less intense interaction between liquid molecules/ions with the solid wall should lead to a smaller transport resistance. With increasing molar concentration, however, the peak position of the dipole angle shifts outwards and more water molecules are driven away from the centerline of the nanotube (figures 7 and 8). Thus, with the presence of more ions, the perturbation is stronger for the motion of water molecules, as well as the Coulomb potential between water molecules/ions, which subsequently leads to more energy consumption to change the dipole angle. As a result, different from the former case, here in a molecular-sized electropolar nanotube the strengthened interaction among water molecules, electrolyte ions and solid wall result in higher shear stress with increased ion concentration.

In brief, variation in the microstructures of water molecules at different levels of confinement accounts for distinct transport behaviors, in terms of the magnitude and varying trend of shear stress with molar concentration of additive electrolytes. In medium and larger nanotubes (e.g. $D \geqslant 2.51$ nm), the ions are surrounded by liquid molecules to form a somewhat stable solvation shell structure, and the intensified electric fields due to additive ions tend to strengthen this stability of the solvation shell as a result of minimizing the systemic energy state, so as to 'compact' the water cluster more closely and lead to more 'ice-like' liquid molecule motion. In a much smaller nanotube (e.g. $D = 0.81$ nm), on the other hand, a chain of liquid molecules is formed and its stability is vulnerable and could be easily broken as the potential field among the liquid molecules in the chain becomes elevated due to the presence of more ions; thus, the process of minimizing system energy disarrays the motion of liquid molecules and intensifies the interaction among liquid molecules and the wall atoms. We believe there is a certain critical size of nanopores, somewhere between 2.0 and 1.0 nm, under which the transition from solvation shell structure to chain structure will be triggered. Further study of the liquid molecule distribution and hydrogen bond kinetics is required to test this hypothesis and will be presented in our future work.

3.2. Nanofluidic behaviors in different electropolar model nanotubes

Various nanoporous materials demonstrate their potential in applications of NEAS, such as zeolite, silica gel and other metal oxide compounds. Thus, quantifying the effects of varying solid tube phases will shed some light on the general behavior of the electropolar solid nanotube. Three systems consisting of ZnO, SiO_2 and Al_2O_3 rigid model nanotubes with smooth surfaces are numerically studied herein; and particularly, for all of these solid systems, effects of loading (transport) rate and molar concentration of electrolyte, which are more controllable in our practice, are numerically analyzed to extract any solid phase dependences.

3.2.1. Rate effect in different solid tubes. The transport rate had been previously identified as a potential factor to affect the nanofluidic properties [18, 34]. In essence, a higher transport rate of liquid molecules over a solid surface leaves the system less time to fully optimize its position and relieve transport stress. The position of the first solvation shell is also closer to the nanotube wall at a higher transport rate, which could lead to a higher resistance as the water molecules continuously overcome energy barriers. The general relationship between the shear stress τ and averaged transport rate $\bar{v}$ follows a power function as $\tau \propto \bar{v}^m$ [18], and such a trend is revealed in figure 9 for three different solid tubes (ZnO, Al_2O_3 and SiO_2 model nanotubes with $D = 2.51$ nm) when the transport rate was varied from ~50 up to ~300 m s^{-1} [18]. For the NaCl/water solution[11] (with a molarity equal to 2.0 M), the variation trends of both the shear stress and effective shear viscosity qualitatively suggest their dependences on the transport rate. The shear stress increases nonlinearly with transport rate, with the power index, m, smaller than 1.0 in all three tubes, suggesting a non-Newtonian shear-thinning phenomenon. Normally, under a bulk situation, the 300 m s^{-1} transport rate would almost make no difference in rheological properties, since the typical flowing timescale (the ratio of

[11] All three alkali chlorides are simulated. The ranking of ionic size of Li^+, Na^+ and K^+ is found to still persist in terms of the effective shear stress. For convenience, we only present the results of the NaCl–water solution.

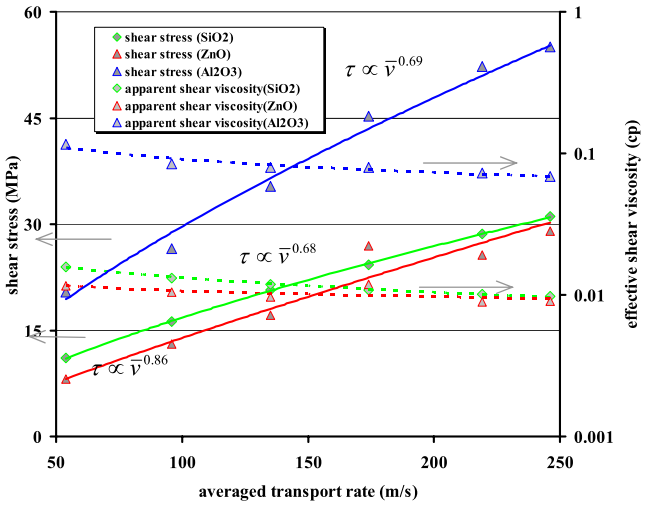

Figure 9. Distributions of shear stress and effective shear viscosity of electrolyte–water solution (NaCl, 2.0 M) in ZnO, Al_2O_3 and SiO_2 model nanotubes with identical dimensions ($D = 2.51$ nm), as functions of averaged transport rate $\bar{v}$.

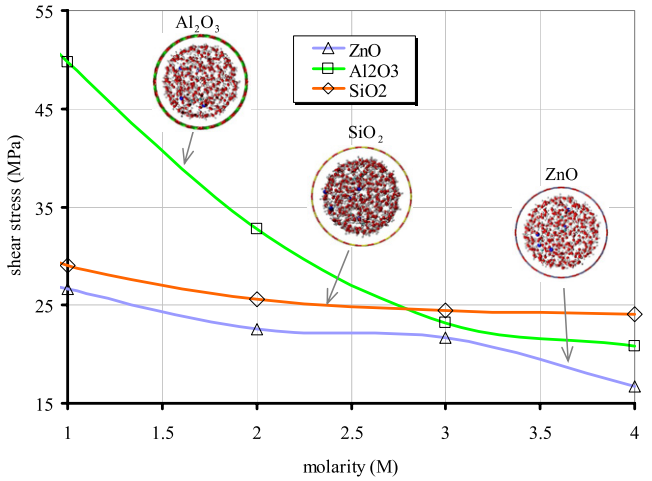

Figure 10. Distribution of shear stress in ZnO, SiO_2 and Al_2O_3 model nanotubes ($D = 2.51$ nm), with the molar concentration of electrolyte (NaCl)–water solution increasing from 1.0 to 4.0 M at the transport rate of ~200 m s^{-1}.

the typical dimension D over transport rate v) is several orders higher than the relaxation time required by water to reach equilibrium under an external disturbance; however, the nanoscale confinement leads to a shearing rate that is 10^9 higher than that of the bulk situation, which greatly shortens the timescale for equilibrium and thus the transport resistance tends to be smaller. On the graph, the effective viscosity $\tilde{\eta}$ is also found to decrease slightly with increasing averaged transport rate $\bar{v}$. Nonetheless, the overall magnitude of $\tilde{\eta}$ is still much smaller than that of bulk pure water for all three solid tubes.

3.2.2. Concentration effect in different solid tubes. Despite the consistent general trend of shear stress versus averaged transport rate for the representative electropolar ZnO, Al_2O_3 and SiO_2 model nanotubes, distinctions still exist in terms of the detailed mechanisms. In figure 9, it is apparent that, for a given liquid flow with constant molarity and dimension of solid nanopores, the magnitude of shear stress and effective shear viscosity in the Al_2O_3 model nanotube are much higher than those encountered in both ZnO and SiO_2 model nanotubes at low electrolyte concentrations. This trend is repeated in figure 10, on which the results of shear stress are given by varying the molar concentration of NaCl/water solution from 1.0 to 4.0 M (while fixing the nanopore diameter and the transport rate at ~200 m s^{-1}). The magnitude of effective shear stress τ in the Al_2O_3 model nanotube is much higher, ~50.0 MPa at 1.0 M, compared with ~29.0 MPa for the SiO_2 model nanotube and ~23.3 MPa for the ZnO model nanotube. The Al_2O_3 model nanotube also has a very strong ion concentration dependence: the effective shear stress drops almost 150% when the molar concentrations of NaCl increases to 4.0 M—and, at that moment, the shear resistance of the Al_2O_3 model nanotube to the NaCl solution is, in fact, lower than that in ZnO and SiO_2 model nanotubes.

The above comparisons show that the variation of solid phases could lead to substantially different characteristics in a nanoenvironment, hence impacting the performances of nanofluidic components, such as NEAS. The different levels of shear stress could imply different wetting capabilities of solid surfaces to the given electrolyte–water solution; the greater non-wetting solid surface facilitates the liquid flow over it. Based on this argument, from figures 9 and 10, Al_2O_3 is implicated to be much more hydrophilic than ZnO and SiO_2 nanotubes (especially for a low concentration of electrolytes). Indeed, in parallel experiments the nanoporous zeolite is found to be hydrophobic, more or less, only when the ratio of SiO_2 to Al_2O_3 exceeds a certain threshold number, e.g. 280 in our test[12]. Otherwise further surface treatment of zeolite or silica nanoporous materials will have to be performed to increase the ratio of silicon dioxide, and thus yield a high intrusion barrier suitable for high-performance NEAS[13].

In previous experiments, it was reported that saturated electrolyte solutions, e.g. NaCl, KCl, can be utilized to modify the intrusion process [39, 60]. In general, the initial intrusion pressure could be favorably elevated via the introduction of electrolyte [40]. Based on the findings in this paper, in a molecular-sized small nanochannel, the increase of electrolyte concentration could also enhance the dissipation via the increased shear stress, and thus it is favorable for promoting the energy dissipation efficiency. In a somewhat larger nanochannel, the decrease of the transport shear stress is relatively mild with increasing electrolyte concentration. In

[12] Note that merely a higher ratio of Si/Al cannot guarantee a zeolite is hydrophobic. Other factors, such as the compensatory cations to balance the charge deficit (resulting from substitution of Al for Si), could be a crucial consideration of hydrophobicity.

[13] The energy absorbed by NEAS is governed by both the initial intrusion pressure of liquid into the nanopore (where a more hydrophobic nanoporous particle surface is more appropriate) and the resistance encountered by the liquid transport (for this purpose a more hydrophilic solid nanopore provides a higher shear resistance for dissipation). The current paper focuses on the second factor and how it varies with material and system parameters. The study on the characteristics of the first factor (intrusion pressure) was reported in some of our other published work [17, 18]. For the overall NEAS design, a balance between the two factors is required.

this case, it is expected that, as the electrolyte concentration is increased, there is competition between the two factors of increasing initial intrusion pressure and decreasing shear stress, leading to a balance of the energy absorption performance of NEAS.

3.2.3. Nanotube size and ionic size effects and implications for NEAS. From the above analyses and comparisons we can learn that, qualitatively, in nanotubes made of different solid materials, the trend for shear stress being affected by the loading (transport) rate and concentration of electrolyte is monotonic and consistent among all solid phases studied. Additional simulations regarding the previously mentioned nanotube size effect, ionic size ranking and the reverse ionic concentration effect were performed and analyzed; and the results, not surprisingly, confirmed that the main conclusions we obtained in the former sections (on the SiO_2 tube) are transferable to other solid phases, such as ZnO and Al_2O_3. This is important for practical applications of nanofluidic components including the optimized design of NEAS—once a nanoporous phase is chosen, the principles revealed in this study could be employed to manipulate the nanofluidic transport behavior, e.g. increasing the system shear stress, by adjusting a number of geometrical and system parameters. For different solid nanotubes, there is some difference among the magnitude of a system's shear stress, which is attributed to the distinct lattice structure and surface charge distribution of the given solid phase. Furthermore, other solid pore characteristics, such as surface roughness and more complicated pore structures, could affect the nanofluidic transport properties, which need to be the subject of future studies.

4. Conclusion

Numerical simulations of the flow of electrolyte/water solution confined in a polar nanotube are carried out to elucidate the mechanisms behind ion transport and shed some light on optimizing the energy dissipation properties using nanomaterials. Due to the strong confinement of the solid nanotube, the system characteristics depend on the tube size, tube phase, concentration of electrolyte and phase of electrolyte, as well as the flow transport rate.

When fixing other system parameters, the system performance shows heavy dependence on the size of nanopores: a bigger size nanotube leads to a higher transport shear stress. If variations in the molar concentration of electrolyte solutions are also considered, the shear stress τ and effective shear viscosity $\tilde{\eta}$ show an opposite trend in a small (molecular-sized) tube than the trend seen in a medium or larger sized nanotube, in which a higher concentration results in decreased shear stress. This reversal of the trend is found to be the result of the distinct molecule/ion microstructure formed inside the smaller and larger nanoenvironments. In addition, larger ion size leads to larger flow resistance. By varying the solid phases, the general nanotube size effect, electrolyte concentration effect and ion size effect are found to be unchanged, although the magnitude of shear stress does change in different solid phase nanotubes. At a higher transport rate, the shear stress goes up, which could be favorable to dissipate energy. Furthermore, the substantial difference in the trend of shear stress with molar concentration of electrolyte in ZnO, SiO_2 and Al_2O_3 nanotubes implies that the Al_2O_3 nanotube is more hydrophilic, which agrees with experimental observations.

These numerical discoveries provide meaningful guidelines for the design of nanofluidic components. For example, inside small nanotubes, especially a molecular-sized polar nanotube, a quasi-one-dimensional chain of water molecules is formed which could serve as a low resistance conductor by taking advantage of the relatively low shear stress during the transport process; however, an increased ionic concentration will weaken the system's transport efficiency. Meanwhile, in a medium or larger sized polar nanotube, although the much stronger transport resistance makes this system ideal for energy dissipation applications, the 'ice-like' smooth transport behaviors under much more 'salty' conditions will debase its performance, calling for the need of a balanced design. Other downsides associated with nanoporous material with larger pore size are the relatively lower transport rate inside a pore under a given external loading and lower inner specific area density ($\propto D^{-1}$) for the specified porosity. Fortunately, these drawbacks could be somewhat overcome by considering the fact that several-fold increases in D can lead to orders of increase in the magnitude of the shear stress and effective viscosity $\tilde{\eta}$; thus high performance of NEAS is still expected [40]. The silicon-dioxide-based nanoporous materials seem to be ideal for energy absorption purposes owing to their ubiquity in the natural world and their relatively hydrophobic surface [39]. Nonetheless, in this case, the portion of impurities, such as Al_2O_3, has to be well engineered to achieve optimum system performance. The much smaller transport resistance of the LiCl solution in ZnO nanotubes suggests they could be used to fabricate nano-energy converters (instead of dissipators). Research investigations in this area could be both inspiring and meaningful.

Acknowledgments

The work is supported by the NSF under grant no. CMMI-0643726 (XC) and CMS-0409521 (PJC). QZ and XC are supported by the National Natural Science Foundation of China (50928601). XC is also supported by a World Class University (WCU) program through the National Research Foundation of Korea funded by the Ministry of Education, Science and Technology of Korea (R32-2008-000-20042-0) and the Changjiang Scholar Program of Ministry of Education of China. YL and XC appreciate funding from the International cooperation project of Tsinghua University (20091081236).

References

[1] Guenes S and Sariciftci N S 2008 Hybrid solar cells *Inorg. Chim. Acta* **361** 581–8
[2] Gyurcsányi R E 2008 Chemically-modified nanopores for sensing *TRAC, Trends Anal. Chem.* **27** 627–39

[3] Healy K, Schiedt B and Morrison A P 2008 Solid-state nanopore technologies for nanopore-based DNA analysis *Nanomedicine* **2** 875–97

[4] Schoch R B, Han J Y and Renaud P 2008 Transport phenomena in nanofluidics *Rev. Mod. Phys.* **80** 839–83

[5] Holtzel A and Tallarek U 2007 Ionic conductance of nanopores in microscale analysis systems: where microfluidics meets nanofluidics *J. Sep. Sci.* **30** 1398–419

[6] Martinac B 2004 Mechanosensitive ion channels: molecules of mechanotransduction *J. Cell Sci.* **117** 2449–60

[7] Tombola F, Pathak M and Isacoff E 2006 How does voltage open an ion channel? *Annu. Rev. Cell Dev. Biol.* **22** 23–52

[8] Chen X, Cui Q, Yoo J, Tang Y and Yethiraj A 2008 Gating mechanisms of mechanosensitive channels of large conductance part I: a continuum mechanics-based hierarchical framework *Biophys. J.* **95** 563

[9] Xu J and Lavan D A 2008 Designing artificial cells to harness the biological ion concentration gradient *Nat. Nanotechnol.* **3** 666–70

[10] Vaitheeswaran S and Thirumalai D 2008 Interactions between amino acid side chains in cylindrical hydrophobic nanopores with applications to peptide stability *Proc. Natl Acad. Sci.* **105** 17636–41

[11] Yernool D, Boudker O, Jin Y and Gouaux E 2004 Structure of a glutamate transporter homologue from Pyrococcus horikoshii *Nature* **431** 723–882

[12] Stein D, Heyden F H J v d, Koopmans W J A and Dekker C 2006 Pressure-driven transport of confined DNA polymers in fluidic channels *Proc. Natl Acad. Sci. USA* **103** 15853–8

[13] Kenis P J A and Stroock A D 2006 Materials for micro- and nanofluidics *MRS Bull.* **31** 87–94

[14] Leary S P, Liu C Y and Apuzzo M L J 2006 Toward the emergence of nanoneurosurgery: part II—nanomedicine: diagnostics and imaging at the nanoscale level *Neurosurgery* **58** 805–23

[15] Chen X, Surani F B, Kong X G, Punyamurtula V K and Qiao Y 2006 Energy absorption performance of a steel tube enhanced by a nanoporous material functionalized liquid *Appl. Phys. Lett.* **89** 241918

[16] Cailliez F, Trzpit M, Soulard M, Demachy I, Boutin A, Patarin J l and Fuchs A H 2008 Thermodynamics of water intrusion in nanoporous hydrophobic solids *Phys. Chem. Chem. Phys.* **10** 4817–26

[17] Liu L, Qiao Y and Chen X 2008 Pressure-driven water infiltration into carbon nanotube: the effect of applied charges *Appl. Phys. Lett.* **92** 101927

[18] Chen X, Cao G, Han A, Punyamurtula V K, Liu L, Culligan P J, Kim T and Qiao Y 2008 Nanoscale fluid transport: size and rate effects *Nano Lett.* **8** 2988–92

[19] Coudert F-X, Cailliez F, Vuilleumier R, Fuchs A H and Boutin A 2008 Water nanodroplets confined in zeolite pores *Phys. Chem. Chem. Phys.* **141** 377–98

[20] Cailliez F, Boutin A, Demachy I and Fuchs A H 2009 Thermodynamic study of water confinement in hydrophobic zeolites by Monte Carlo simulations *Mol. Simul.* **35** 24–30

[21] Bellat J-P, Paulin C, Jeffroy M, Boutin A, Paillaud J-L, Patarin J, Lella A D and Fuchs A H 2009 Unusual hysteresis loop in the adsorption–desorption of water in NaY zeolite at very low pressure *J. Phys. Chem.* C **113** 8287–95

[22] Marry V, Rotenberg B and Turq P 2008 Structure and dynamics of water at a clay surface from molecular dynamics simulation *Phys. Chem. Chem. Phys.* **10** 4802–13

[23] Han A and Qiao Y 2007 Controlling infiltration pressure of a nanoporous silica gel via surface treatment *Chem. Lett.* **36** 882–3

[24] Stein D, Kruithof M and Dekker C 2004 Surface-charge-governed ion transport in nanofluidic channels *Phys. Rev. Lett.* **93** 035901

[25] Formasiero F, Park H G, Holt J K, Stadermann M, Grigoropoulos C P, Noy A and Bakajin O 2008 Ion exclusion by sub-2 nm carbon nanotube pores *Proc. Natl Acad. Sci.* **105** 17250–5

[26] Han A, Lu W, Punyamurtula V K, Chen X, Surani F B, Kim T and Qiao Y 2008 Effective viscosity of glycerin in a nanoporous silica gel *J. Appl. Phys.* **104** 124906

[27] Guriyanova S and Bonaccurso E 2008 Influence of wettability and surface charge on the interaction between an aqueous electrolyte solution and a solid surface *Phys. Chem. Chem. Phys.* **10** 4871–8

[28] Huang D M, Cottin-Bizonne C, Ybert C and Bocquet L 2008 Aqueous electrolytes near hydrophobic surfaces: dynamic effects of ion specificity and hydrodynamic slip *Langmuir* **24** 1442–50

[29] Cao G, Qiao Y, Zhou Q and Chen X 2008 Water infiltration behaviours in carbon nanotubes under quasi-static and dynamic loading conditions *Mol. Simul.* **34** 1267–74

[30] Qiao Y, Cao G and Chen X 2007 Effects of gas molecules on nanofluidic behaviors *J. Am. Chem. Soc.* **129** 2355–9

[31] Rauscher M and Dietrich S 2008 Wetting phenomena in nanofluidics *Annu. Rev. Mater. Res.* **38** 143–72

[32] Majumder M, Chopra N, Andrews R and Hinds B J 2005 Nanoscale hydrodynamics: enhanced flow in carbon nanotubes *Nature* **438** 44

[33] Hummer G, Rasaiah J C and Noworyta J P 2001 Water conduction through the hydrophobic channel of a carbon nanotube *Nature* **414** 188–90

[34] Zhao J, Qiao Y, Culligan P J and Chen X 2010 Confined liquid flow in nanotube: a numerical study and implications for energy absorption *J. Comput. Theor. Nanosci.* **7** 379–87

[35] Bouzigues C I, Tabeling P and Bocquet L 2008 Nanofluidics in the Debye layer at hydrophilic and hydrophobic surfaces *Phys. Rev. Lett.* **101** 114503

[36] Liu L, Chen X, Lu W, Han A and Qiao Y 2009 Infiltration of electrolytes in molecular-sized nanopores *Phys. Rev. Lett.* **102** 184501

[37] Song C M, Yan Z F and Lu M 2002 Synthesis and characterization of super-surface MCM-41 zeolites *Acta Phys.-Chim. Sin.* **18** 279–83

[38] Chen N Y, Degnan T F and Smith C M 1994 *Molecular Transport and Reaction in Zeolites* (New York: Wiley)

[39] Han A and Qiao Y 2007 Effects of surface treatment of a MCM-41 on motions of confined liquids *J. Phys. D: Appl. Phys.* **40** 5743–6

[40] Han A, Chen X and Qiao Y 2008 Effects of the addition of electrolyte on liquid infiltration in a hydrophobic nanoporous silica gel *Langmuir* **24** 7044–7

[41] MacKerell A D Jr, Bashford D, Bellott M, Dunbrack R L Jr, Evanseck J D, Field M J, Fischer S, Gao J, Guo H, Ha S, Joseph-McCarthy D, Kuchnir L, Kuczera K, Lau F T K, Mattos C, Michnick S, Ngo T, Nguyen D T, Prodhom B, Reiher W E, Roux B I, Schlenkrich M, Smith J C, Stote R, Straub J, Watanabe M, Wiórkiewicz-Kuczera J, Yin D and Karplus M 1998 All-atom empirical potential for molecular modeling and dynamics studies of proteins *J. Phys. Chem.* B **102** 3586–616

[42] Jorgensen W L, Chandrasekhar J, Madura J D, Impey R W and Klein M L 1983 *J. Chem. Phys.* **79** 926–35

[43] Lim T-C 2003 The relationship between Lennard-Jones (12-6) and Morse potential functions *Z. Naturf.* a **58** 615–7

[44] Hockney R and Eastwood J 1981 *Computer Simulation Using Particles* (Bristol, PA: Taylor and Francis)

[45] Pettitt B M 1986 Alkali halides in water: ion–solvent correlations and ion–ion potentials of mean force at infinite dilution *J. Chem. Phys.* **84** 5836–44

[46] Kornherr A, French S A, Sokol A A, Catlow C R A, Hansal S, Hansal W E G, Besenhard J O, Kronberger H, Nauer G E and Zifferer G 2004 Interaction of adsorbed organosilanes with polar zinc oxide surfaces: a molecular dynamics study comparing two models for the metal oxide surface *Chem. Phys. Lett.* **393** 107–11

[47] Halicioglu T and Pound G M 1975 Calculation of potential energy parameters from crystalline state properties *Phys. Status Solidi* a **30** 619

[48] Bartolotti L J, Pedersen L G and Charifson P S 1991 Long range nonbonded attractive constants for some charged atoms *J. Comput. Chem.* **12** 1125–8
[49] Chen X, Hutchinson J W and Evans A G 2005 The mechanics of indentation induced lateral cracking *J. Am. Ceram. Soc.* **88** 1233–8
[50] Plimpton S J 1995 Fast parallel algorithms for short-range molecular dynamics *J. Chem. Phys.* **117** 1–19
[51] http://lammps.sandia.gov
[52] Vaitheeswaran S, Rasaiah J C and Hummer G 2004 Electric field and temperature effects on water in the narrow nonpolar pores of carbon nanotubes *J. Chem. Phys.* **121** 7955–65
[53] Han A, Punyamurtula V K, Kim T and Qiao Y 2009 The dependence of infiltration pressure and volume in zeolite Y on potassium chloride concentration *Smart Mater. Struct.* **18** 024005
[54] Jorgensen W L and Madura J D 1985 Temperature and size dependence for Monte Carlo simulations of TIP4P water *Mol. Phys.* **56** 1381–92
[55] Jeffrey G A 1997 *An Introduction to Hydrogen Bonding* (*Topics in Physical Chemistry*) (Oxford: Oxford University Press)
[56] Qiao R and Aluru N R 2005 Atomistic simulation of KCl transport in charged silicon nanochannels: interfacial effects *Colloids Surf.* A **267** 103–9
[57] White J A, Schwegler E, Galli G and Gygi F O 2000 The solvation of Na^+ in water: first-principles simulations *J. Chem. Phys.* **113** 4668–73
[58] Zwolak M, Lagerqvist J and Ventra M D 2009 Quantized ionic conductance in nanopores *Phys. Rev. Lett.* **103** 128102
[59] Gong X, Li J, Zhang H, Wan R, Lu H, Wang S and Fang H 2008 Enhancement of water permeation across a nanochannel by the structure outside the channel *Phys. Rev. Lett.* **101** 257801–4
[60] Han A and Qiao Y 2007 Infiltration pressure of a nanoporous liquid spring modified by an electrolyte *J. Mater. Res.* **22** 644–8